Multiframe Super-Resolution Employing a Spatially Weighted Total Variation Model

Qiangqiang Yuan, Liangpei Zhang, *Senior Member, IEEE,* and Huanfeng Shen, *Member, IEEE*

***Abstract*—Total variation (TV) has been used as a popular and effective image prior model in regularization-based image processing fields, such as denoising, deblurring, super-resolution (SR), and others, because of its ability to preserve edges. However, as the TV model favors a piecewise constant solution, the processing results in the flat regions of the image being poor, and it cannot automatically balance the processing strength between different spatial property regions in the image. In this paper, we propose a spatially weighted TV image SR algorithm, in which the spatial information distributed in different image regions is added to constrain the SR process. A newly proposed and effective spatial information indicator called difference curvature is used to identify the spatial property of each pixel, and a weighted parameter determined by the difference curvature information is added to constrain the regularization strength of the TV regularization at each pixel. Meanwhile, a majorization–minimization algorithm is used to optimize the proposed spatially weighted TV SR model. Finally, a significant amount of simulated and real data experimental results show that the proposed spatially weighted TV SR algorithm not only efficiently reduces the "artifacts" produced with a TV model in fat regions of the image, but also preserves the edge information, and the reconstruction results are less sensitive to the regularization parameters than the TV model, because of the consideration of the spatial information constraint.**

***Index Terms*—Majorization–minimization (MM), spatially weighted, super-resolution (SR), total variation (TV).**

I. Introduction

HIGH-RESOLUTION (HR) imagery plays a key role in many diverse areas of application, such as medical imaging [1], remote sensing [2], and video surveillance [3], [4]. The traditional methods of obtaining HR images mainly depend on the hardware aspect, for example, increasing the chip size or reducing the pixel size. However, reducing pixel size will lead to an increase in the shot noise, and increasing the chip size will be followed by an increase in capacitance. In addition, the high cost for high-precision optics and image sensors is also an important concern in many commercial applications regarding HR imaging [5]. Consequently, researchers have explored new techniques to produce HR images from one or multiple frames of low-resolution (LR) imagery, a technique that is called super-resolution (SR) technology.

Manuscript received March 15, 2011; revised June 7, 2011; accepted July 11, 2011. Date of publication August 1, 2011; date of current version March 7, 2012. This work was supported in part by the National Basic Research Program of China (973 Program), under Grant 2011CB707105, by the National Natural Science Foundation of China, under Grants 40930532, 41071269, 4080118, and 40971220, and by the Open Research Fund of Key Laboratory of Digital Earth, Center for Earth Observation and Digital Earth, Chinese Academy of Sciences, under Grant 2010LDE006. This paper was recommended by Associate Editor R. Lukac.

Q. Yuan and L. Zhang are with the State Key Laboratory of Information Engineering in Surveying, Mapping, and Remote Sensing, Wuhan University, Wuhan 430070, China (e-mail: yqiang86@gmail.com; zlp62@public.wh.hb.cn).

H. Shen is with the School of Resources and Environmental Science, Wuhan University, Wuhan 430070, China (e-mail: shenhf@whu.edu.cn).

Color versions of one or more of the figures in this paper are available online at http://ieeexplore.ieee.org.

Digital Object Identifier 10.1109/TCSVT.2011.2163447

A. Problem Formulation

Assume that a HR image x is sub-pixel shifted, blurred, down-sampled and has some additive noise and produces a sequence of LR images y_k (Fig. 1). By far the most common forward model for the problem of SR is linear in the form

$$y_k = D_k B_k M_k x + n_k \quad k = 1,\ 2,\ \ldots,\ p \tag{1}$$

where y_k is the kth LR image rearranged in lexicographic order, and which has the size of $L_1 L_2 \times 1$, and x is the original HR image which is also rearranged in lexicographic order, and which has the size of $H_1 H_2 \times 1$. M_k stands for the warp matrix with size $H_1 H_2 \times H_1 H_2$, B_k is the blurring matrix with size $H_1 H_2 \times H_1 H_2$, D_k is the down-sampling matrix with size $L_1 L_2 \times H_1 H_2$, and n_k is the noise vector with size $L_1 L_2 \times 1$. In this paper, we assume that the down-sample matrix D_k and blurring matrix B_k remain the same between the LR images.

The purpose of multiple-frame SR reconstruction is how to accurately reconstruct the HR image x from sequences of LR images y_k.

B. Previous Algorithm

The multiple-frame SR problem was first tackled by Tsai and Huang to enhance the resolution of multitemporal Landsat TM images in the frequency domain [6]. After their work, many frequency domain methods were developed [7], [8]. However, although frequency domain methods are computationally attractive, they have some limitations. For example, it is difficult to incorporate the prior information about HR images using frequency domain methods. For this reason, many spatial domain reconstruction methods have been developed in recent decades, including the nonuniform interpolation approach [9], [10], iterative back-projection approach [11], [12], projection onto convex sets approach [13], [14], maximum likelihood approach [15], maximum *a posteriori* (MAP) approach [16], [17], joint MAP approach [18]–[21], and the hybrid approach [22]. Recently, some SR algorithms without

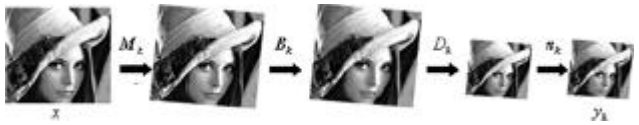

Fig. 1. Degradation process of the HR image.

explicit motion estimation using the non-local means [23] and kernel regression theory [24], [25] have been proposed, and excellent SR results were produced, especially when complex motions are contained in the LR image sequences. In addition, wavelet domain SR methods have also been proposed [26], [27]. Some reviews of the state of the art of SR methods can be found in [5] and [28]–[31].

Assuming that the noise of each LR image is zero-mean Gaussian noise, and each LR frame is independent, the solution model of the SR problem can be represented by the following regularization-based least-squares problem [32]:

$$\hat{x} = \arg\min \left\{ \sum_{k=1}^{p} \| y_k - DBM_k x \|_2^2 + \lambda U(x) \right\}. \qquad (2)$$

In (2), $\sum_{k=1}^{p} \| y_k - DBM_k x \|_2^2$ is the data fidelity item, which stands for the fidelity between the observed LR images and the original HR image, $U(x)$ is the regularization, which gives a prior model of the HR image x, and λ is the regularization parameter, which controls the tradeoff between the data fidelity and prior items.

The regularization item $U(x)$ in (2) plays a very important role in the SR reconstruction process. It controls the perturbation of the solution, solves the ill-posed problem for SR reconstruction, and guarantees a stable HR estimation. In past decades, many regularization models have been proposed, such as Tikhonov regularization [33], Gaussian Markov random fields regularization [34], Huber-MRF regularization [16], [35], weighted-MRF regularization [4], total variation (TV) regularization [36]–[38], bilateral TV (BTV) regularization [28], locally adaptive BTV model [39] and sparse directional regularization [40], amongst others. Recently, the sparse representation-based prior models have been proposed and shown very promising image restoration and SR results [41], [42].

Among the prior models, the TV model is a popular and effective regularization model because of its ability to preserve edge information. However, the TV regularization model also has some shortcomings. One of them is that the TV model favors a piecewise constant solution, which causes the processing result in the flat regions of the image to be poor, and some spatial features, such as textures and small details, are often diminished with noise. Although the noise in the flat regions can be reduced by adjusting the regularization parameter to a large value, the edge and texture information will be blurred. Another drawback is although the TV regularization model is convex, it is not differentiable and is nonlinear. Therefore, it is difficult to optimize it with some popular linear optimization algorithms.

C. Proposed Algorithm

To overcome the aforementioned shortcomings of TV regularization-based SR, in this paper, we propose a spatial information weighted TV (SWTV) SR algorithm. The basic theory of the proposed algorithm can be summarized as follows. An effective spatial information extractor called difference curvature, recently proposed by Chen *et al*. [43] is used to extract the spatial information in the HR image. For each pixel, a weighted parameter determined by the spatial information is added to constrain the TV regularization strength. For flat area pixels, a large weighted parameter is set to suppress noise. On the contrary, for nonsmooth area pixels, a small weighted parameter is set to preserve edge and detailed information. To make the SWTV regularization easy to optimize, the majorization–minimization (MM) approach, which was first proposed in [44], and developed into the image restoration and SR domain in [45]–[48], is used to optimize the SWTV SR model. With the MM approach, the nonquadratic SWTV model minimization problem is converted to successive quadratic minimization problems and is then easy to optimize with some popular linear optimization algorithms, such as conjugate gradient (CG). Another contribution that should be noted in this paper is that we first try to use two blind image quality assessment indices to give an objective assessment of the SR results when the original HR image is unknown. To the best of our knowledge, no one has yet given a blind assessment on the SR reconstruction results when the original HR image is unknown. We think this is very important because the quality assessment, just from the visual aspect, is not sufficient to illustrate the worth of the reconstruction results.

It is noted that although some spatially adaptive TV models have been proposed before [43], [49], they are all used in image denoising problem. As compared with the image denoising problem, the multiframe SR is more complex, which is a process including image denoising, deblurring, and upsampling, we think it is valuable and important to consider the spatial information constraint in the mutiframe SR problem, and it is the first time a spatially weighted TV multiframe SR algorithm has been proposed. The spatial information adaptive process has been integrated into the minimization–majorization process, and the spatial information is updated in each minimization–majorization iteration, which will give a better spatial information extraction result and makes the algorithm more robust.

D. Organization of This Paper

The remainder of this paper is organized as follows. In Section II, our spatially weighted TV regularization SR algorithm is presented in detail. The MM optimization method is described in Section III. In Section IV, some experimental results and discussion are presented and, finally, conclusions are drawn in Section V.

II. Spatially Weighted TV SR

In this section, our spatially weighted TV SR algorithm is presented. First, the TV model is revised, and then the spatially weighted TV model is introduced.

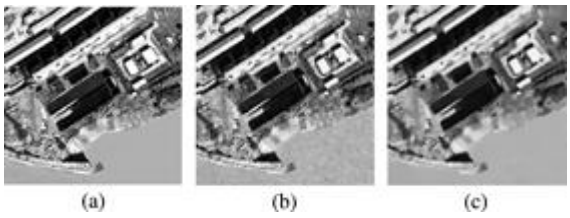

Fig. 2. SR results with different TV regularization strengths. (a) Original HR image. (b) Best (with the highest PSNR value) TV SR result. (c) TV SR result with large regularization strength.

A. TV Model

The TV model was first proposed by Rudin *et al*. [36] in image denoising, because of its advantages in preserving edge and detailed information. For the HR image x, the TV model can be defined as follows:

$$TV(x) = \sum_i \sqrt{\left(\Delta_i^h x\right)^2 + \left(\Delta_i^v x\right)^2} \tag{3}$$

where Δ_i^h and Δ_i^v are linear operators corresponding to horizontal and vertical first-order differences, respectively. At pixel i, $\Delta_i^h x = x_i - x_{r(i)}$, $\Delta_i^v x = x_i - x_{b(i)}$, where $r(i)$ and $b(i)$ represent the nearest neighbor to the right, and below the pixel, respectively.

Although the TV regularization has the advantages of preserving edge and detailed information in the SR process, the processing results in the flat region of the HR image are poor and some "staircase effects" are produced in the flat area [Fig. 2(b)]. Despite that, the noise in the flat regions can be significantly reduced by adjusting the regularization parameter λ to a large value, but the edge and texture information will be blurred [Fig. 2(c)].

From the above phenomenon, it is shown that the regularization λ in the TV model is spatially dependent. Therefore, our spatially weighted TV regularization model considers the spatial dependent property of the TV regularization, will be introduced in detail next.

B. Spatially Weighted TV Regularization

A very critical process in the realization of the spatially weighted TV regularization is how to select a good spatial information indicator, which can better detect the edge information. Traditional spatial information indicators are mostly based on the image gradient (first derivative), which cannot effectively distinguish between edges and ramps. Therefore, in this paper a spatial information indicator based on the second derivative, which is called difference curvature, recently proposed by Chen *et al*. [42] is used, and it has been proved that this indictor can effectively distinguish edges from flat and ramp areas.

For the ith pixel in the image, the difference curvature C_i is defined as follows:

$$C_i = \left| \left| u_{\eta\eta} \right| - \left| u_{\varepsilon\varepsilon} \right| \right| \tag{4}$$

$$u_{\eta\eta} = \frac{\mu_x^2 \mu_{xx} + 2\mu_x \mu_y \mu_{xy} + \mu_y^2 \mu_{yy}}{\mu_x^2 + \mu_y^2} \tag{5}$$

$$u_{\varepsilon\varepsilon} = \frac{\mu_y^2 \mu_{xx} - 2\mu_x \mu_y \mu_{xy} + \mu_x^2 \mu_{yy}}{\mu_x^2 + \mu_y^2} \tag{6}$$

and where η and ε are the direction of the gradient and the direction perpendicular to the gradient. In (5) and (6), μ_x, μ_y, μ_{xx}, μ_{yy}, and μ_{xy} stand for the first and second derivative gradient information of the pixel, respectively. $|\ |$ denotes the absolute value operator.

With the spatial information extraction result using difference curvature, the definition process of the spatially weighted TV regularization can be described as follows.

First, a spatially weighted matrix Wg is defined using the difference curvature, which has the following formation:

$$Wg = \begin{bmatrix} Wg_1 & 0 & \cdots & 0 \\ 0 & Wg_2 & \cdots & 0 \\ \vdots & \vdots & \ddots & \vdots \\ 0 & 0 & \cdots & Wg_{H_1 \times H_2} \end{bmatrix} \tag{7}$$

where Wg_i is the spatial weight of the ith pixel in the high-resolution image, and can be defined with the difference curvature indicator as follows:

$$Wg_i = \frac{1}{1 + \beta C_i} \tag{8}$$

where C_i is the difference curvature value of pixel i, β is the contrast factor. With the spatially weighted matrix Wg, the spatially weighted TV model proposed in this paper can be defined as follows:

$$\begin{aligned} SWTV(x) &= Wg \times TV(x) \\ &= Wg \times \sum_i \sqrt{\left(\Delta_i^h x\right)^2 + \left(\Delta_i^v x\right)^2}. \end{aligned} \tag{9}$$

From (8) and (9), it is clearly seen that for the pixels in smooth areas, because the C_i value is close to zero, Wg_i is close to 1, which means that a large TV regularization strength is enforced to these pixels, and then the noise in the flat and ramp regions will be well suppressed. Conversely, for edge and texture pixels, because the C_i value is very large, Wg_i is small and almost close to zero, and this means that a weak TV regularization strength is enforced to these pixels, so the edge and texture will be well preserved.

Substituting $U(x)$ in (2) by $SWTV(x)$, presented in (9), the cost function used in this paper can be written as follows:

$$\hat{x} = \arg\min \left\{ \sum_{i=1}^{p} \| y_k - DBM_k x \|_2^2 + \lambda(SWTV(x)) \right\}. \tag{10}$$

According to the analysis above, it is shown that the spatially weighted TV SR model can automatically adjust the contribution of the data fidelity item and the TV prior item with the spatial information distributed differently at each pixel, which causes it to effectively reduce the noise in flat regions, and at the same time, preserve the edge and texture information.

III. MM Optimization

The main idea of the MM optimization approach is to replace the traditional nonquadratic function with a quadratic and differentiable upper bound (majorizer) equation, and then the optimization of the nonquadratic function can be replaced with the iterative optimization of the majorizer equation.

To accomplish the MM idea on the SWTV SR model, we first consider the following relationship:

$$\sqrt{ab} \le \frac{a+b}{2} \rightarrow \sqrt{a} \le \frac{a+b}{2\sqrt{b}}\ . \tag{11}$$

Let $b = \left(\Delta_i^h x^m\right)^2 + \left(\Delta_i^v x^m\right)^2$, $a = \left(\Delta_i^h x\right)^2 + \left(\Delta_i^v x\right)^2$, applying (11) to the SWTV model presented in (9), the majorizer equation can be defined as follows:

$$G_{SWTV}(x|x^m) = Wg \times \left\{ \begin{matrix} \frac{1}{2}\sum_i \frac{\left(\Delta_i^h x\right)^2 + \left(\Delta_i^v x\right)^2}{\sqrt{\left(\Delta_i^h x^m\right)^2 + \left(\Delta_i^v x^m\right)^2}} + \\ \frac{1}{2}\sum_i \frac{\left(\Delta_i^h x^m\right)^2 + \left(\Delta_i^v x^m\right)^2}{\sqrt{\left(\Delta_i^h x^m\right)^2 + \left(\Delta_i^v x^m\right)^2}} \end{matrix} \right\}. \tag{12}$$

Define w_i^m, which has the formation

$$w_i^m = \frac{1}{\sqrt{\left(\Delta_i^h x^m\right)^2 + \left(\Delta_i^v x^m\right)^2}}. \tag{13}$$

The final majorizer equation can be defined as [46]

$$G_{SWTV}(x|x^m) = Wg \times \left\{(Rx)^T W^m (Rx)\right\} \tag{14}$$

where $R = \begin{bmatrix} R^h \\ R^v \end{bmatrix}$, $W^m = \begin{bmatrix} \Lambda^m & \\ & \Lambda^m \end{bmatrix}$, $\Lambda^m = diag(w_i^m)$.

R^h and R^v represent two matrices that have the size of $H_1H_2 \times H_1H_2$, such that $R^h x$ and $R^v x$ are the first-order difference of x.

Incorporating (14) into (10) and replacing $SWTV(x)$ with $G_{SWTV}(x|x^m)$, the final majorizer function of (10) can be written as follows:

$$\begin{aligned} G(x|x^m) = \{&\sum_{k=1}^{p} \|y_k - DBM_k x\|_2^2 + \\ &\lambda \times Wg \times ((Rx)^T W^m (Rx))\}. \end{aligned} \tag{15}$$

For the majorizer function (15), because it is quadratic and differentiable, minimization to x leads to the following linear system:

$$\begin{aligned} &\left(\sum_{k=1}^{p} (DBM_k)^T (DBM_k) + \lambda \times (Wg \times ((Rx)^T W^m (Rx))\right) x^{(m+1)} \\ &= \sum_{k=1}^{p} (DBM_k)^T y_k. \end{aligned} \tag{16}$$

For (16), the CG algorithm can be used to optimize it. In each iteration, the spatially weighted parameter Wg_i is adaptively updated, with the purpose of extracting a more accurate spatial information distribution. Finally, the optimization procedure is concluded as follows.

Algorithm 1 MM based SWTV super-resolution algorithm

Initial the reconstruction image with the **bilinear interpolated** image $x^{(0)}$;
Compute $\sum_{k=1}^{p}(DBM_k)^T y_k$ and $\sum_{k=1}^{p}(DBM_k)^T(DBM_k)$,
iteration number $m = 0$
While "MM stopping criterion"
not satisfied **do**
  Compute W^m according (20)
  Setting $x^{m+1} = x^m$;
  While x^{m+1} does not satisfy " CG stopping criterion" **do**
  Compute spatially weighted parameter
    Wg_i **according (11) with** x^{m+1}
    x^{m+1} = CG iteration for system
    Update Wg_i according (11) with x^{m+1}
end **While**
$m = m + 1$;
end **While**

IV. Experimental Results and Discussion

In this section, the experimental results with the proposed SWTV SR model, and some analysis and discussion are presented.

A. Experimental Setting

Seven data sets were used to test the performance of the proposed SWTV SR method. The first three experiments were three simulated experiments with known HR images and the following four experiments were the real data experiments. In all experiments, the motion model is assumed to be the global translational model.

In this paper, in the simulated experiments, we use the peak signal-to-noise ratio (PSNR), the structural similarity (SSIM) [50], [51], and a promising recently proposed full-reference image quality assessment index called FSIM [52], to evaluate the reconstruction results.

In the real data experiments, because the original HR image was not obtained, the reconstruction results cannot be accessed with the PSNR and SSIM indices. Therefore, the blind image quality index (BIQI) proposed recently in [53], and the non-referenced image quality assessment index Q-metric proposed recently in [54], are used to give an objective assessment of the reconstruction results. To the best of our knowledge, this is the first time a blind assessment of the SR reconstruction results has been undertaken when the true HR image cannot be obtained. For these two indices, the higher the value, the better the image quality.

To assess the relative merits of the proposed methodology, we compare the proposed algorithm with Tikhonov regularization, BTV regularization [28] and TV regularization [37], in the simulated data experiments, while adding the comparison of the bilinear interpolation (BI) results in the experiment without the original HR image.

The termination condition of the CG procedure is set to be 1e-5, and the termination condition of the MM procedure is also set to be 1e-5. The resolution enhancement factor is set

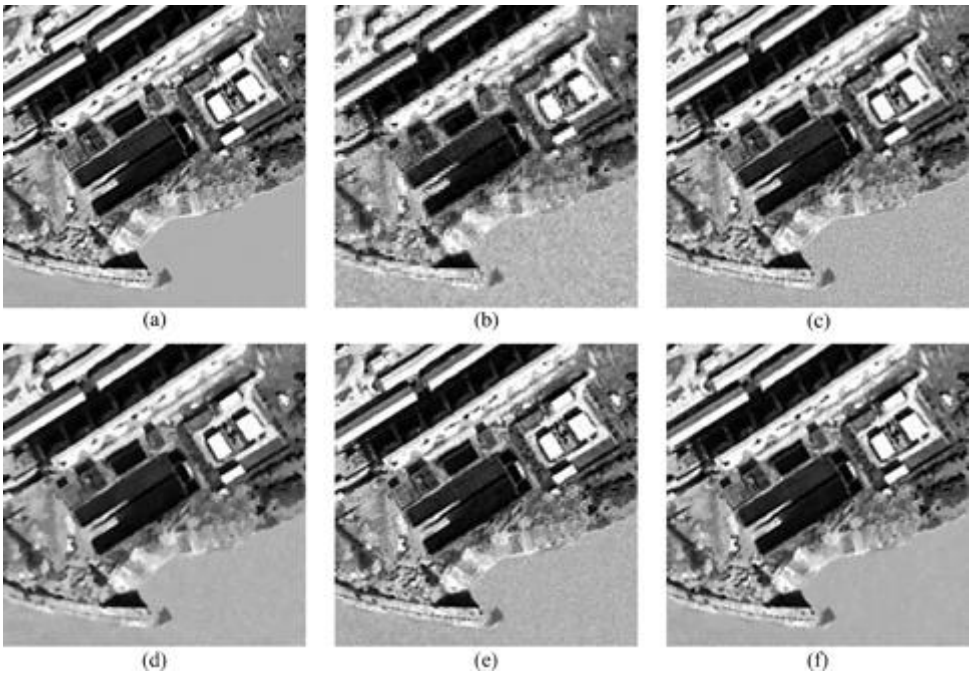

Fig. 3. Reconstruction results of the "aerial" image. (a) Original HR image. (b) LR image. (c) Tikhonov regularization. (d) BTV regularization. (e) TV regularization. (f) SWTV regularization.

to be 2 in all the experiments. The regularization parameter and other parameters in all the prior models are adjusted until the best SR result is obtained. For the simulated experiments, the best result is selected to be the one with the highest PSNR value, and for the real data experiments, the best result is selected to be the one with the highest Q metric value [54].

B. Experimental Results

1) *Simulated Experiments:* In the simulated experiments, the four original HR images used are, respectively, the "aerial" image with the size of 200×200, the "spot 5" image with the size of 256×256, and the "cameraman" image with the size of 200×200. In the simulated process, with the degradation mode described in Section I-A, the HR image was first shifted with sub-pixel displacements to produce four images. The sequence was then convoluted with a PSF of 5*5 window size and unit variance, and down-sampled with a factor 2 in both the vertical and horizontal directions. Finally, zero-mean Gaussian noise was added to the sequence.

The reconstruction results of the simulated experiments are presented in Figs. 3, 5, and 7. In these figures, (a) is the original HR image, (b) is one of the down-sampled LR images, and (c) shows the Tikhonov regularization model SR result. The reconstruction results of the BTV regularization model, TV regularization model, and the proposed SWTV regularization model are, respectively, shown in (d)–(f). The detailed regions cropped from these three figures are, respectively, presented in Figs. 4, 6, and 8. The PSNR, SSIM values, and FSIM values of the different algorithms are presented in Table I.

Among the four SR algorithms, it is shown that the proposed SWTV regularization model produces a better SR result. In the edge area, the detailed information is well preserved, while in the smooth area, the high-intensity noise is better suppressed. However, for the other three regularization models, because the spatial information constraint is not considered in the SR process, and an equal regularization strength is used in the whole HR image, they cannot automatically adjust the regularization strength between different spatial property regions in the image, and the tradeoff among edge preserving, deblurring, and denoising cannot be adaptively balanced in different HR image regions. Consequently, it is shown that some noise still remains in the flat regions of the SR results.

TABLE I
PSNR, SSIM, AND FSIM VALUES OF DIFFERENT RECONSTRUCTION METHODS IN SIMULATED EXPERIMENTS

	Assessment Index	Tikhonov	BTV	TV	SWTV
Aerial	PSNR (DB)	28.514	32.003	33.199	33.413
	SSIM	0.86237	0.88253	0.89465	0.9379
	FSIM	0.93323	0.9434	0.95384	0.95346
Spot 5	PSNR (DB)	27.209	31.415	32.460	32.636
	SSIM	0.88661	0.87006	0.90565	0.92432
	FSIM	0.95675	0.9471	0.95808	0.95811
Cameraman	PSNR (DB)	26.806	27.788	28.3777	28.65210
	SSIM	0.72531	0.80399	0.90299	0.90653
	FSIM	0.89357	0.92598	0.94358	0.94217

The good performance of the proposed SWTV regularization model can also be illustrated by the PSNR, SSIM, and FSIM values presented in Table I. It is shown that the SWTV regularization produces the highest PSNR value, and also has the highest SSIM value, which illustrates that the proposed SWTV regularization SR algorithm produces a better reconstruction result, close to the original HR image, both from gray value and image structure aspects. Although for the FSIM index, the evaluation values in the "aerial" image

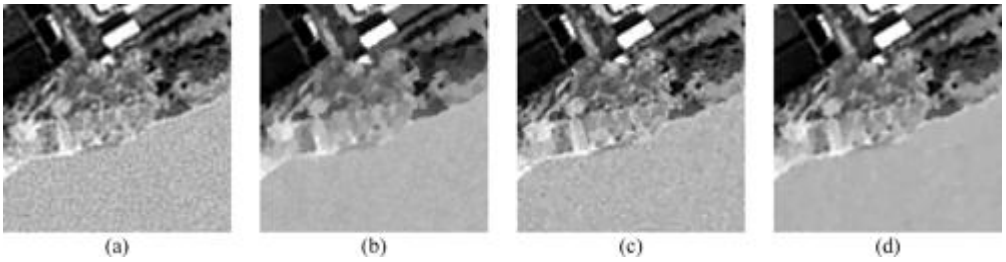

Fig. 4. Detailed flat regions cropped from Fig. 3. (a) Tikhonov regularization. (b) BTV regularization. (c) TV regularization. (d) SWTV regularization.

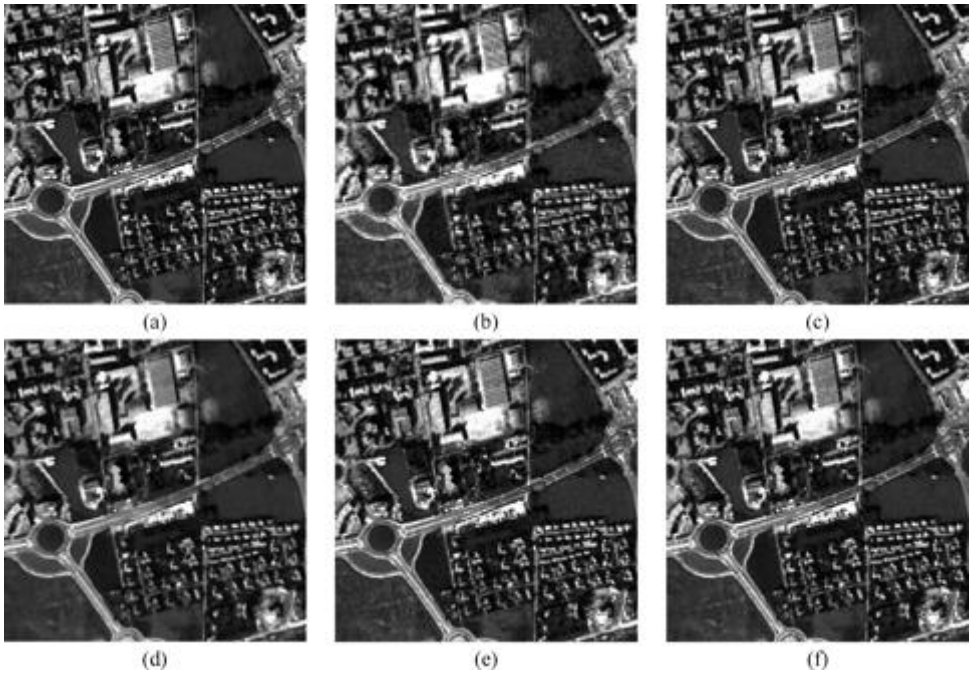

Fig. 5. Reconstruction results of "spot5" image. (a) Original HR image. (b) LR image. (c) Tikhonov regularization. (d) BTV regularization. (e) TV regularization. (f) SWTV regularization.

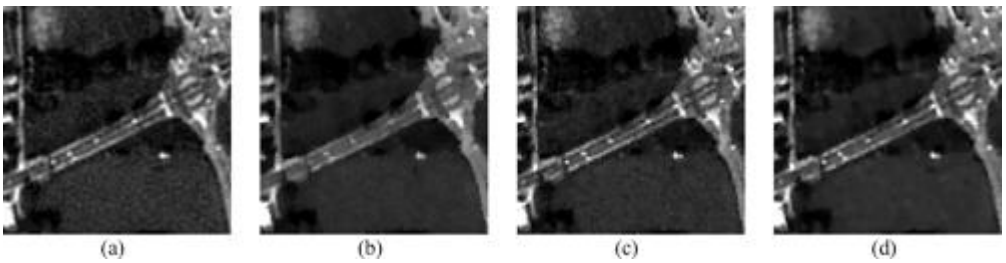

Fig. 6. Detailed regions cropped from Fig. 5. (a) Tikhonov regularization. (b) BTV regularization. (c) TV regularization. (d) SWTV regularization.

and the "cameraman" image are slightly lower than the TV model, the beneficial effect of the proposed algorithm can be particularly seen in the visual effect, especially in the detailed regions presented in Figs. 4, 6, and 8.

In (8), a parameter β is used to define the spatial information weighted parameter Wg_i, and the parameter β controls the ability of the parameter Wg_i to distinguish the edge and texture area from the flat and ramp area. To show the effect of the different parameter β on the SR result, in Table II we give the PSNR and SSIM value when β is selected to be 0.005, 0.01, 0.05, 0.1, 0.5, and 1, respectively.

TABLE II
PSNR AND SSIM VALUES WITH DIFFERENT β VALUES IN EXPERIMENT 1

β	0.005	0.01	0.05	0.1	0.5	1
PSNR (DB)	33.383	33.316	33.413	33.32	33.223	33.303
SSIM	0.93633	0.93545	0.93779	0.93817	0.9370	0.9349

It can be seen in Table II that the PSNR and SSIM values show little change with the change of the parameter β. Therefore, in this paper, for all the experiments, the parameter β is set to be 0.05.

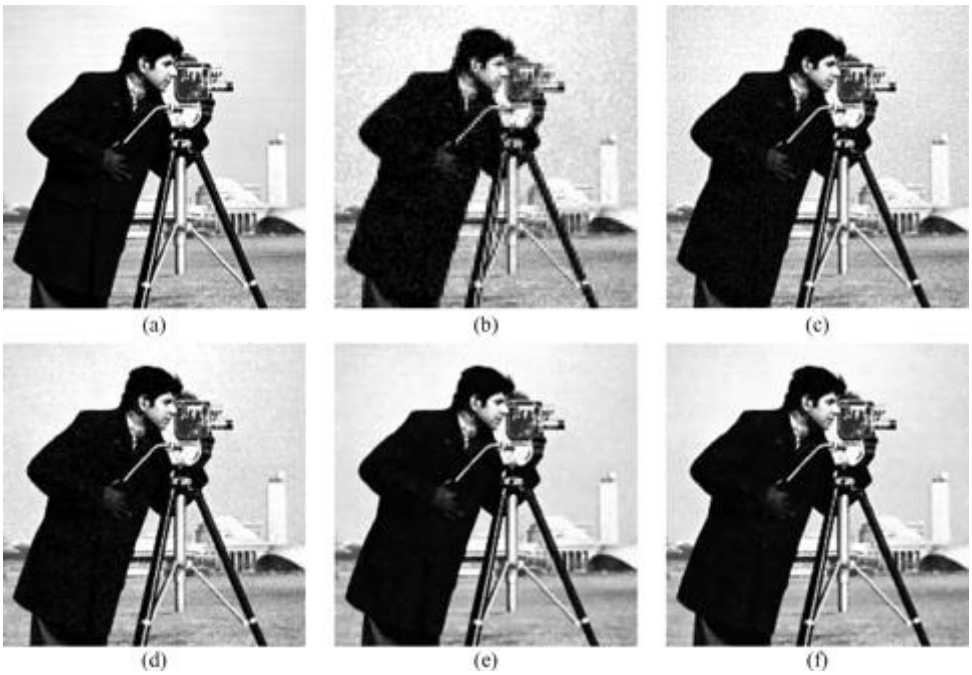

Fig. 7. Reconstruction results of "cameraman" image. (a) Original HR image. (b) LR image. (c) Tikhonov regularization. (d) BTV regularization. (e) TV regularization. (f) SWTV regularization.

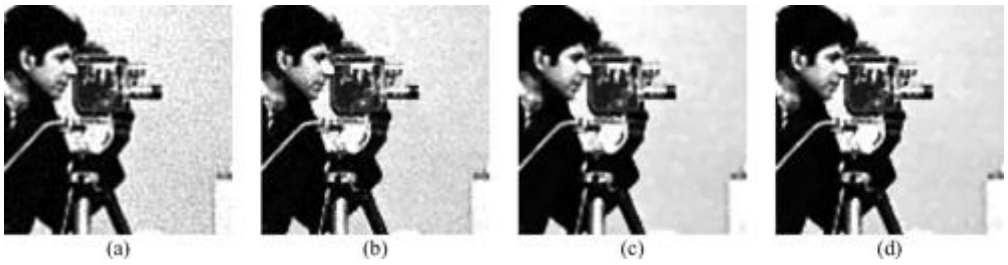

Fig. 8. Detailed regions cropped from Fig. 7. (a) Original HR image. (b) LR image. (c) Tikhonov regularization. (d) BTV regularization. (e) TV regularization. (f) SWTV regularization.

2) *Real Data Experiments:* In the real data experiments, four real data sets obtained from the Multidimensional Signal Processing Research Group of UCSC [55] are used to verify the proposed algorithm. In order to reduce the computational load, we just select the first ten frames in the four real data sets for our experiment. The well-performing registration approach presented in [56] and [57] is used as the motion estimation method.

The reconstruction results of these four real data sets are, respectively, shown in Figs. 9–15. In these figures, (a) is one frame of the LR image sequence, (b) is the bilinear interpolation results; the reconstruction results using Tikhonov regularization, BTV regularization, and TV regularization are shown in (c)–(e), respectively; and (f) presents the proposed SWTV reconstruction result.

From these figures, it is shown that the resolution of the image has certainly increased after using the SR technique, compared with the results of the BI results. In the Tikhonov regularization SR result, noise is not suppressed thoroughly, and some noise is still present in the flat regions. For the BTV regularization-based SR reconstruction result, although the noise is suppressed to some extent, the detailed information, such as the number "200" in the HR image of the "EIA" image and the letter "color" in the "disk" sequences, is not well preserved. In the TV regularization SR reconstruction result, although the edge and detailed information is well maintained, noise in the flat regions is not well suppressed and some "artifacts" are produced. In the proposed SWTV

TABLE III
BIQI AND Q-METRIC VALUES OF DIFFERENT RECONSTRUCTION METHODS IN REAL DATA EXPERIMENTS

LR Sequence	Assessment Index	Tikhonov	BTV	TV	SWTV
EIA	BIQI	33.342	68.155	71.683	**90.218**
	Q-metric	201.0	180.01	215.63	**241.62**
Surveillance	BIQI	26.14	16.725	39.069	**45.85**
	Q-metric	163.85	128.30	166.25	**170.38**
Alpaca	BIQI	72.124	42.939	**57.98**	56.14
	Q-metric	160.83	119.36	147.735	**163.45**
Disk	BIQI	93.364	67.571	92.312	**109.24**
	Q-metric	122.90	86.793	123.47	**131.92**

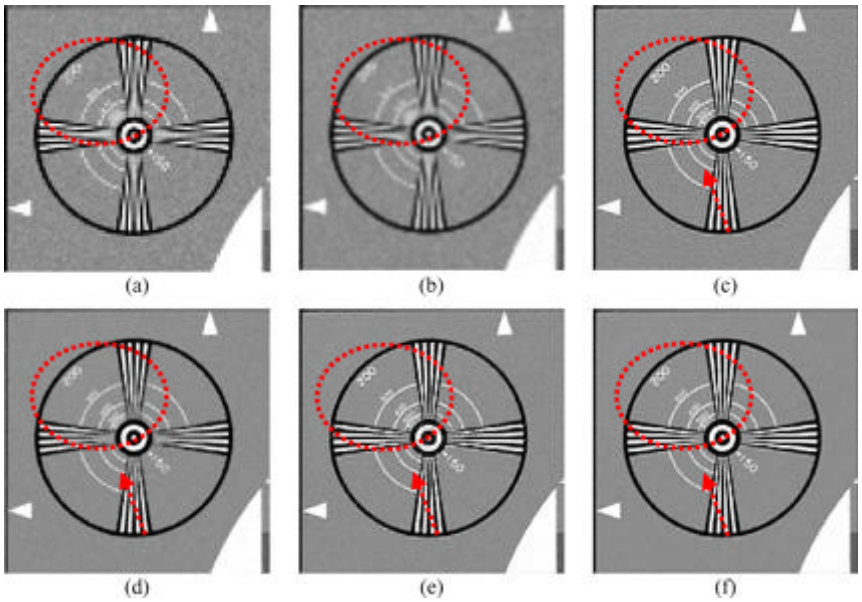

Fig. 9. Reconstruction results of the "EIA" image sequence. (a) LR image. (b) Bilinear interpolation. (c) Tikhonov regularization. (d) BTV regularization. (e) TV regularization. (f) SWTV regularization.

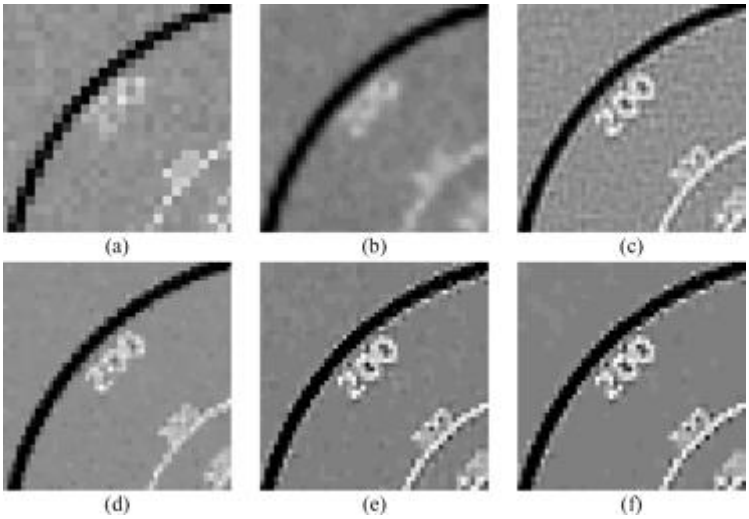

Fig. 10. Detailed regions cropped from Fig. 9. (a) LR image. (b) Bilinear interpolation. (c) Tikhonov regularization. (d) BTV regularization. (e) TV regularization. (f) SWTV regularization.

TABLE IV
BIQI AND Q-METRIC VALUES OF DIFFERENT RECONSTRUCTION METHODS I ''EIA'' EXPERIMENT WHEN THE REGULARIZATION PARAMETER $\lambda = 20$

Assessment Index	TV	**SWTV**
BIQI	99.407	**99.692**
Q-metric	210.97	**237.58**

regularization reconstruction result, not only is noise in flat regions well reduced, but also the edge information is better preserved than with the other three reconstruction methods.

The assessment results are shown in Table III. It can be seen that the proposed SWTV regularization produces almost all of the highest BIQI values and Q-metric values, which is consistent with the visual effect presented in Figs. 9–15.

C. Discussion

1) *Robustness with Different Noise Intensity:* To validate the robustness of the proposed SWTV regularization model with changes in the noise intensity, in Fig. 16(a) and (b), we give two plots which present the change of the PSNR value with different noise variance, from 0.001 to 0.005, in simulated experiments 1 and 2, respectively. From the two figures, it is shown that the proposed SWTV regularization model is robust with regard to changes in the noise level and produces higher PSNR values than the TV regularization under different noise intensity.

2) *Robustness with Regularization Parameter λ:* In the SR model presented in (2), the regularization parameter λ plays a very important role. It controls the relative contribution of the data fidelity item and the prior model item. If the value selected

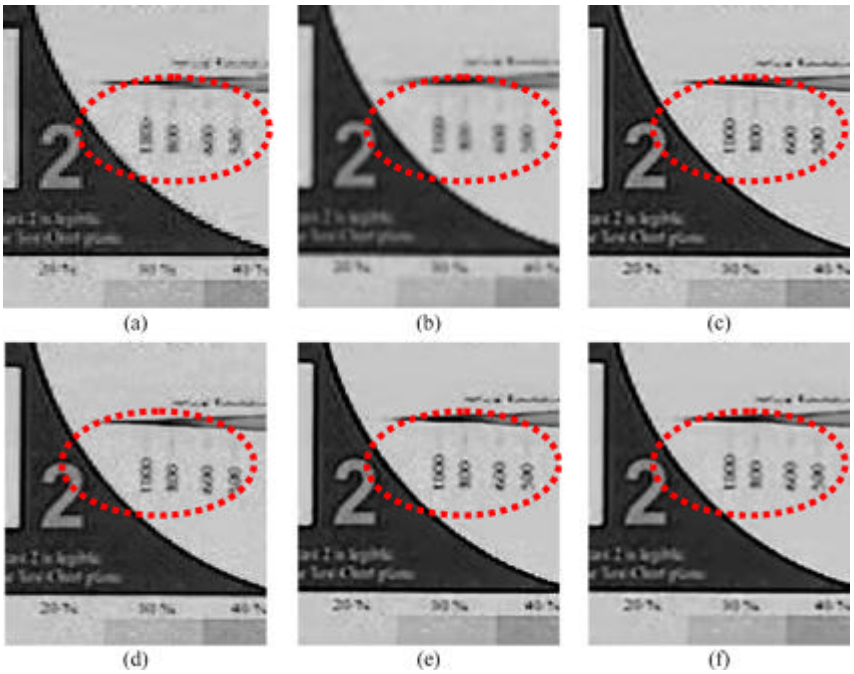

Fig. 11. Reconstruction results of the "surveillance" video sequence. (a) LR image. (b) Bilinear interpolation. (c) Tikhonov regularization. (d) BTV regularization. (e) TV regularization. (f) SWTV regularization.

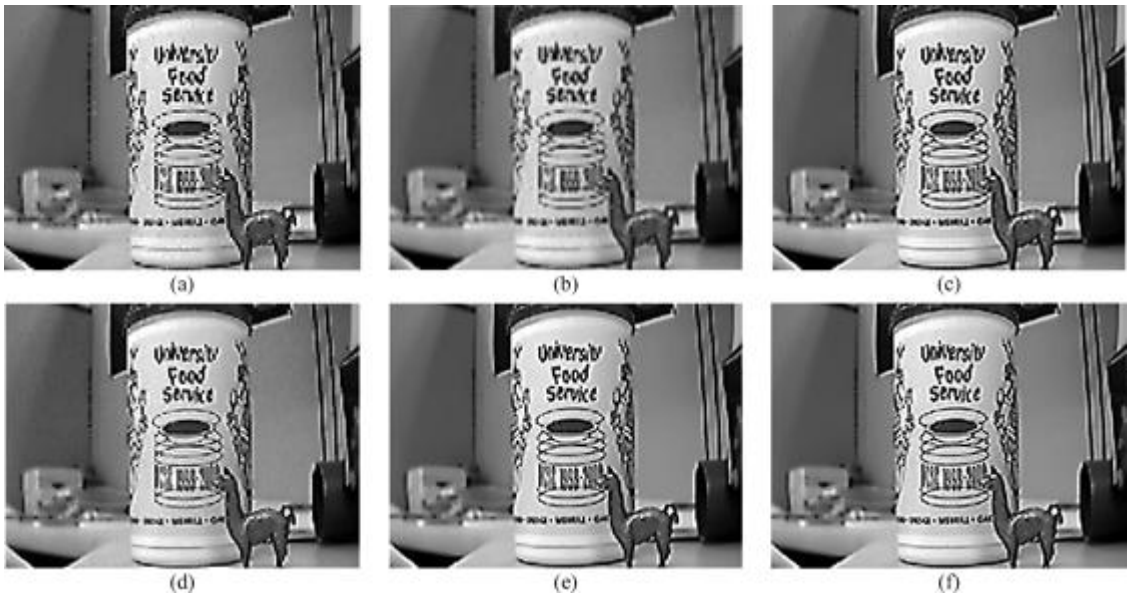

Fig. 12. Reconstruction results of the "alpaca" video sequence. (a) LR image. (b) Bilinear interpolation. (c) Tikhonov regularization. (d) BTV regularization. (e) TV regularization. (f) SWTV regularization.

is too small, the noise will not be well suppressed; inversely, if the value selected is too large, the reconstruction result will be blurred. However, in the proposed SWTV SR model in (10), because the spatial information distribution in the HR image is added to constrain the regularization strength of the TV model, the reconstruction results are not so sensitive to the change of regularization λ. To show the robustness of the proposed SWTV regularization with the regularization parameter λ and the effectiveness of the spatial information constraint, we plot the change of the PSNR value versus the change of the parameter λ in simulated experiment 1 and experiment 2, as shown in Fig. 17(a) and (b), and the plot of the change of PSNR value versus the change of regularization parameter λ in the TV regularization is also presented to give a comparison. From the two plots, it is shown that the proposed SWTV regularization is robust with the change of the parameter λ to a large value, and the PSNR value remains little changed when the regularization parameter is set to be a large value. However, for the traditional TV regularization, the change of the regularization parameter λ has a very large effect on the reconstruction results. In particular, the PSNR value decreases sharply when the regularization parameter becomes large.

Fig. 13. Detailed regions cropped from Fig. 12. (a) LR image. (b) Bilinear interpolation. (c) Tikhonov regularization. (d) BTV regularization. (e) TV regularization. (f) SWTV regularization.

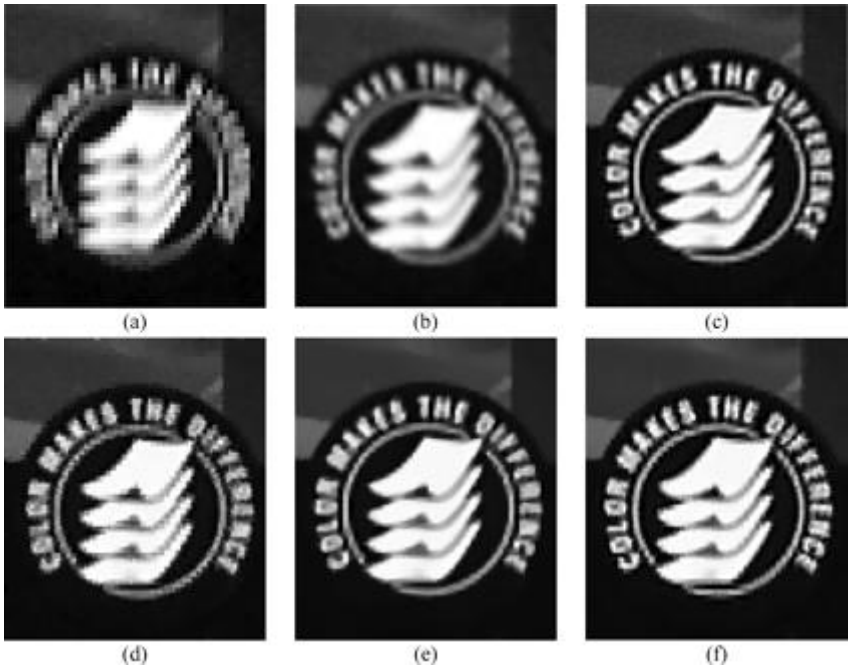

Fig. 14. Reconstruction results of the "disk" video sequence. (a) LR image. (b) Bilinear interpolation. (c) Tikhonov regularization. (d) BTV regularization. (e) TV regularization. (f) SWTV regularization.

The robustness with the regularization parameter and the effectiveness of the spatial information constraint can also be illustrated in Fig. 18, which presents the SR results when a very large regularization parameter ($\lambda = 20$) is used in the TV regularization and SWTV regularization in the "EIA" sequences experiment, and the reconstruction results are, respectively, presented in Fig. 18(a) and (b). It is shown that the SWTV regularization gives a clearer result when a very large regularization parameter ($\lambda = 20$) is used, which illustrates that a good SR result can be had with the SWTV model, even if the regularization parameter λ is selected to be a large value. However, for the TV model, when the regularization parameter becomes too large, the SR result looks too blurred. The objective assessment of the reconstruction results in Fig. 18 is presented in Table IV. It shows that the SWTV SR result has a higher BIQI value and Q-metric value, which is consistent with the visual effects shown in Fig. 18.

The comparison above illustrates the effectiveness of the spatial information constraint; the consideration of the spatial information constraint is very necessary in the SR reconstruction process.

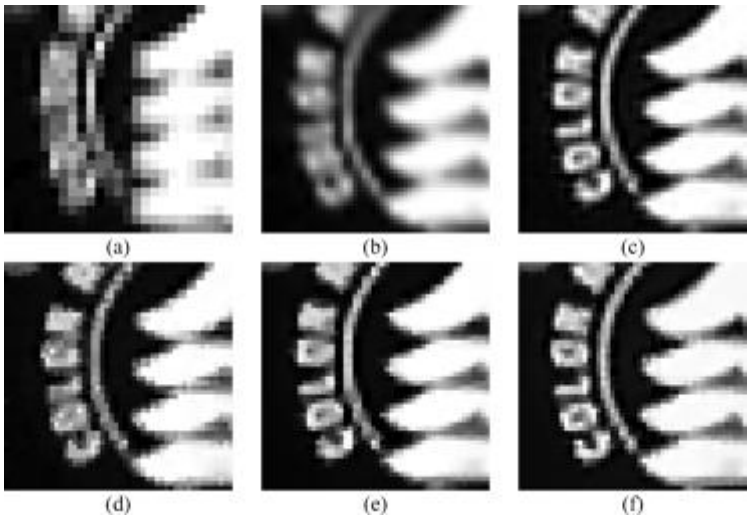

Fig. 15. Detailed regions cropped from Fig. 14. (a) LR image. (b) Bilinear interpolation. (c) Tikhonov regularization. (d) BTV regularization. (e) TV regularization. (f) SWTV regularization.

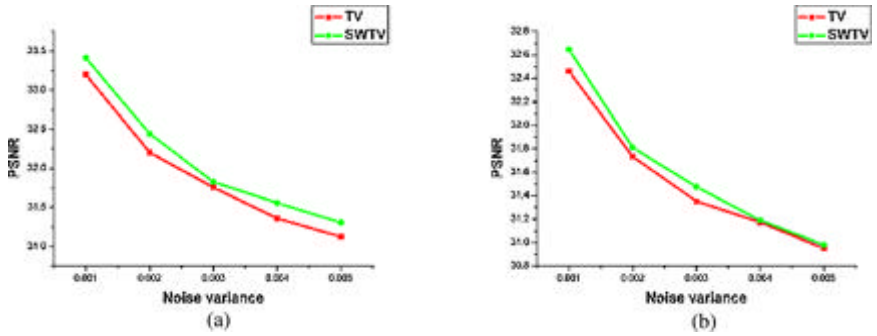

Fig. 16. Change of the PSNR value with different noise levels, for TV regularization and SWTV regularization. (a) Simulated experiment 1. (b) Simulated experiment 2.

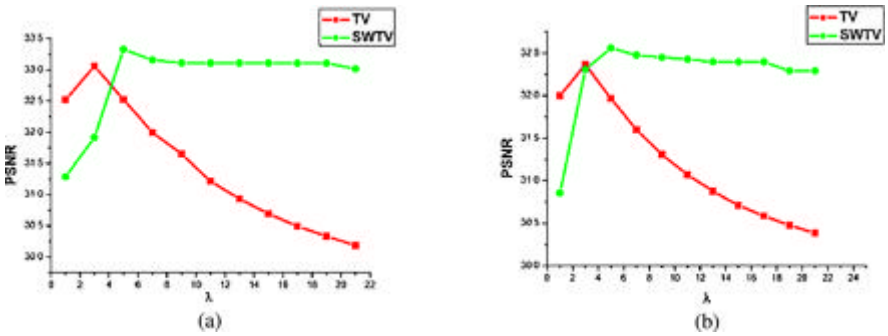

Fig. 17. Change of the PSNR value versus the regularization parameter λ in TV regularization and SWTV regularization. (a) Simulated experiment 1. (b) Simulated experiment 2.

3) *A Comparison Between Difference Curvature and Gradient:* In this paper, a newly proposed spatial information extractor called difference curvature is used to detect the spatial information distribution in the image and construct the SWTV model. In this part, to show the better performance of the difference curvature in constructing the SWTV model, compared to the gradient information (first derivative), we plot the reconstruction PSNR value using the difference curvature-based SWTV model and image gradient-based SWTV model, in simulated experiments 1 and 2, respectively, under different regularization parameters. The comparison results are shown in Fig. 19(a) and (b); (a) is the comparison in simulated experiment 1 and (b) is the comparison in simulated experiment 2.

From the two plots, it is shown that the difference curvature spatial information extractor presents a better SR performance than the image gradient, under different regularization parameter settings. The reason is that the difference curvature has better ability to discriminate edge and texture information with flat and ramp information, and it is more robust with noise to extract spatial information than the image gradient.

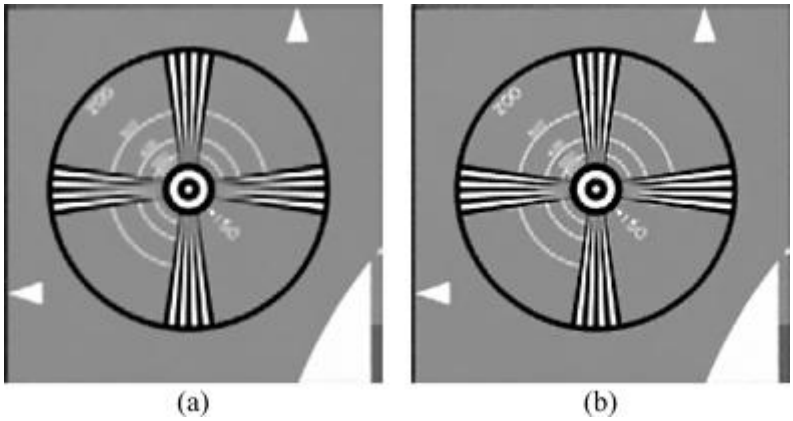

Fig. 18. Reconstruction results of the "EIA" image sequences using a large parameter $\lambda = 20$. (a) TV regularization. (b) SWTV regularization.

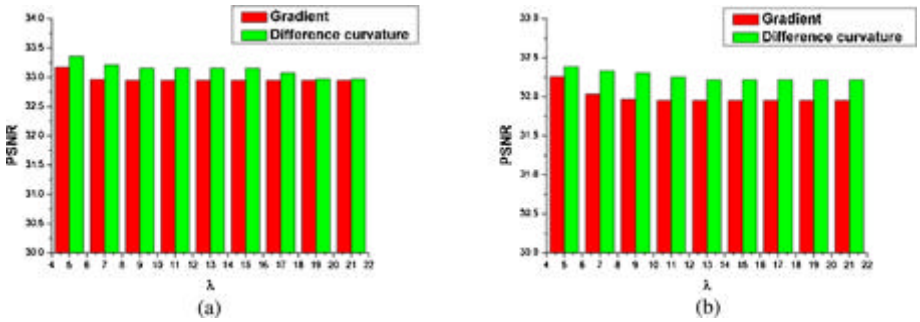

Fig. 19. Comparison of the performance of difference curvature and image gradient with different regularization parameters. (a) Simulated experiment 1. (b) Simulated experiment 2.

V. Conclusion

In this paper, we proposed a SWTV regularization-based SR algorithm. The spatial information extracted by a newly proposed difference curvature edge indicator is used to constrain the SR reconstruction process. For the flat region, large TV regularization is enforced to reduce noise; for the edge area, a small TV regularization is enforced to preserve the edge and detailed information. Also, the MM algorithm is used to optimize the SWTV SR model. Experimental results presented in Section V illustrate that the presented SWTV regularization not only efficiently reduces the noise in the flat regions, but also effectively preserves the edge and detailed information. Finally, some discussion and analysis about the experiment results are also presented, which demonstrate that the proposed SWTV regularization model is robust with changes in the noise level, and less sensitive to the regularization parameter λ, because of the consideration of the spatial information constraint.

While the proposed spatially weighted SR method can be improved from some aspects, such as the considering of a more complex motion model, and combining with the sparse representation prior model in [41] and [42], and others, which will be on our future research agenda.

Acknowledgment

The authors would like to thank the editors and the anonymous reviewers for their valuable suggestions. They also would like to thank Prof. P. Milanfar and M. Elad for providing the BTV SR code, and the real experiment data.

References

[1] A. Martin, A. Gotlieb, and R. Henkelman, "High-resolution MR imaging of human arteries," *J. Magn. Resonance Imaging*, vol. 5, no. 1, pp. 93–100, 1995.

[2] X. Huang, L. Zhang, and P. Li, "Classification and extraction of spatial features in urban areas using high-resolution multispectral imagery," *IEEE Geosci. Remote Sensing Lett.*, vol. 4, no. 2, pp. 260–264, Apr. 2007.

[3] C. Wang, P. Xue, and W. Lin, "Improved super-resolution reconstruction from video," *IEEE Trans. Circuits Syst. Video Technol.*, vol. 16, no. 11, pp. 1411–1422, Nov. 2006.

[4] L. Zhang, H. Zhang, H. Shen, and P. Li, "A super-resolution reconstruction algorithm for surveillance images," *Signal Process.*, vol. 90, no. 3, pp. 848–859, 2010.

[5] S. Park, M. Park, and M. Kang, "Super-resolution image reconstruction: A technical overview," *IEEE Signal Process. Mag.*, vol. 20, no. 3, pp. 21–36, May 2003.

[6] R. Tsai and T. Huang, "Multiple frame image restoration and registration," *Adv. Comput. Vis. Image Process.*, vol. 1, no. 2, pp. 317–339, 1984.

[7] S. Kim, N. Bose, and H. Valenzuela, "Recursive reconstruction of high resolution image from noisy undersampled multiframes," *IEEE Trans. Acoust. Speech Signal Process.*, vol. 38, no. 6, pp. 1013–1027, Jun. 1990.

[8] S. Kim and W. Su, "Recursive high-resolution reconstruction of blurred multiframe images," *IEEE Trans. Image Process.*, vol. 2, no. 4, pp. 534–539, Oct. 1993.

[9] H. Ur and D. Gross, "Improved resolution from sub-pixel shifted pictures," *CVGIP Graph. Models Image Process.*, vol. 54, no. 2, pp. 181–186, 1992.

[10] M. Alam, J. Bognar, R. Hardie, and B. Yasuda, "Infrared image registration and high-resolution reconstruction using multiple translationally shifted aliased video frames," *IEEE Trans. Instrum. Meas.*, vol. 49, no. 5, pp. 915–923, Oct. 2000.

[11] M. Irani and S. Peleg, "Improving resolution by image registration," *CVGIP Graph. Models Image Process.*, vol. 53, no. 3, pp. 231–239, 1991.
[12] M. Irani and S. Peleg, "Motion analysis for image enhancement resolution, occlusion, and transparency," *J. Vis. Commun. Image Representation*, vol. 4, no. 4, pp. 324–335, 1993.
[13] H. Stark and P. Oskoui, "High resolution image recovery from image-plane arrays, using convex projections," *J. Opt. Soc. Amer. A*, vol. 6, no. 11, pp. 1715–1726, 1989.
[14] A. Patti, M. Sezan, and A. Tekalp, "Super resolution video reconstruction with arbitrary sampling lattices and nonzero aperture time," *IEEE Trans. Image Process.*, vol. 6, no. 8, pp. 1064–1076, Aug. 1997.
[15] B. Tom and A. Katsaggelos, "Reconstruction of a high-resolution image by simultaneous registration, restoration, and interpolation of low-resolution images," in *Proc. IEEE Int. Conf. Image Process.*, vol. 2. Oct. 1995, pp. 539–542.
[16] R. Schultz and R. Stevenson, "Extraction of high-resolution frames from video sequences," *IEEE Trans. Image Process.*, vol. 5, no. 6, pp. 996–1011, Jun. 1996.
[17] S. Belekos, N. Galatsanos, and A. Katsaggelos, "Maximum *a posteriori* video super-resolution using a new multichannel image prior," *IEEE Trans. Image Process.*, vol. 19, no. 6, pp. 1451–1464, Jun. 2010.
[18] R. Hardie, K. Barnard, and E. Armstrong, "Joint MAP registration and high-resolution image estimation using a sequence of undersampled images," *IEEE Trans. Image Process.*, vol. 6, no. 12, pp. 1621–1633, Dec. 1997.
[19] H. Shen, L. Zhang, B. Huang, and P. Li, "A MAP approach for joint motion estimation, segmentation and super-resolution," *IEEE Trans. Image Process.*, vol. 16, no. 2, pp. 479–490, Feb. 2007.
[20] H. Zhang, L. Zhang, H. Shen, and P. Li, "A MAP approach for joint image registration, blur identification and super resolution," in *Proc. 5th Int. Conf. Image Graph.*, Sep. 2009, pp. 97–102.
[21] M. Zibetti and J. Mayer, "A robust and computationally efficient simultaneous super-resolution scheme for image sequences," *IEEE Trans. Circuits Syst. Video Technol.*, vol. 17, no. 10, pp. 1288–1300, Oct. 2007.
[22] M. Elad and A. Feuer, "Restoration of a single super resolution image from several blurred, noisy, and undersampled measured images," *IEEE Trans. Image Process.*, vol. 6, no. 12, pp. 1646–1658, Dec. 1997.
[23] M. Protter, M. Elad, H. Takeda, and P. Milanfar, "Generalizing the nonlocal-means to super-resolution reconstruction," *IEEE Trans. Image Process.*, vol. 18, no. 1, pp. 36–51, Jan. 2009.
[24] H. Takeda, S. Farsiu, and P. Milanfar, "Kernel regression for image processing and reconstruction," *IEEE Trans. Image Process.*, vol. 16, no. 2, pp. 349–366, Feb. 2007.
[25] H. Takeda, P. Milanfar, M. Protter, and M. Elad, "Super-resolution without explicit subpixel motion estimation," *IEEE Trans. Image Process.*, vol. 18, no. 9, pp. 1958–1975, Sep. 2009.
[26] N. Nguyen and P. Milanfar, "A wavelet-based interpolation restoration method for superresolution (wavelet superresolution)," *Circuits Syst. Signal Process.*, vol. 19, no. 4, pp. 321–338, 2000.
[27] J. Hui and C. Fermuller, "Robust wavelet-based super-resolution reconstruction: Theory and algorithm," *IEEE Trans. Pattern Anal. Mach. Intell.*, vol. 31, no. 4, pp. 649–660, Apr. 2009.
[28] S. Farsiu, M. Robinson, M. Elad, and P. Milanfar, "Fast and robust multiframe super-resolution," *IEEE Trans. Image Process.*, vol. 13, no. 10, pp. 1327–1344, Oct. 2004.
[29] S. Farsiu, M. D. Robinson, M. Elad, and P. Milanfar, "Advances and challenges in super-resolution," *Int. J. Imaging Syst. Technol.*, vol. 14, no. 2, pp. 47–57, 2004.
[30] A. K. Katsaggelos, R. Molina, and J. Mateos, *Super Resolution of Images and Video*, 1st ed. San Rafael, CA: Morgan and Claypool, 2007.
[31] P. Milanfar, *Super Resolution Imaging*, 1st ed. Boca Raton, FL: CRC Press, 2010.
[32] Q. Yuan, L. Zhang, H. Shen, and P. Li, "Adaptive multiple-frame image super-resolution based on U-curve," *IEEE Trans. Image Process.*, vol. 19, no. 12, pp. 3157–3170, Dec. 2010.
[33] X. Zhang, E. Lam, E. Wu, and K. Wong, "Application of Tikhonov regularization to super-resolution reconstruction of brain MRI images," in *Proc. Medical Imaging Informatics*, Aug. 2007, pp. 46–51.
[34] A. Kanemura, S. Maeda, and S. Ishii, "Superresolution with compound Markov random fields via the variational EM algorithm," *Neural Netw.*, vol. 22, no. 7, pp. 1025–1034, 2009.
[35] H. Shen, M. K. Ng, P. Li, and L. Zhang, "Super-resolution reconstruction algorithm to MODIS remote sensing images," *Comput. J.*, vol. 52, no. 1, pp. 90–100, 2009.
[36] L. Rudin, S. Osher, and E Fatemi, "Nonlinear total variation based noise removal algorithms," *Phys. D Nonlinear Phenomena*, vol. 60, no. 1, pp. 259–268, 1992.
[37] M. Ng, H. Shen, E. Lam, and L. Zhang, "A total variation regularization based super-resolution reconstruction algorithm for digital video," *EURASIP J. Adv. Signal Process.*, vol. 2007, no. 74585, pp. 1–16, 2007.
[38] A. Marquina and S. Osher, "Image super-resolution by TV-regularization and Bregman iteration," *J. Sci. Comput.*, vol. 37, no. 3, pp. 367–382, 2008.
[39] X. Li, Y. Hu, and X. B. Gao, "A multiframe image super resolution method," *Signal Process.*, vol. 90, no. 2, pp. 405–414, 2010.
[40] Y. Li, D. Dai, and L. Shen, "Multiframe super-resolution reconstruction using sparse directional regularization," *IEEE Trans. Circuits Syst. Video Technol.*, vol. 20, no. 7, pp. 945–956, Jul. 2010.
[41] W. Dong, L. Zhang, G. Shi, and X. Wu, "Image deblurring and supper-resolution by adaptive sparse domain selection and adaptive regularization," *IEEE Trans. Image Process.*, vol. 20, no. 7, pp. 1838–1857, Jul. 2011.
[42] W. Dong, X. Li, L. Zhang, and G. Shi, "Sparsity-based image denoising via dictionary learning and structural clustering," in *Proc. CVPR*, 2011, pp. 1–8.
[43] Q. Chen, P. Montesinos, Q. Sun, P. Heng, and D. Xia, "Adaptive total variation denoising based on difference curvature," *Image Vis. Comput.*, vol. 28, no. 3, pp. 298–306, 2010.
[44] D. Hunter and K. Lange, "A tutorial on MM algorithms," *Amer. Statist.*, vol. 58, no. 2, pp. 30–37, Feb. 2004.
[45] J. Bioucas-Dias, M. Figueiredoand, and J. Oliveira, "Adaptive total-variation image deconvolution: A majorization–minimization approach," in *Proc. EUSIPCO*, Sep. 2006, pp. 1–4.
[46] J. Bioucas-Dias, M. Figueiredo, and J. Oliveira, "Total variation image deconvolution: A majorization–minimization approach," in *Proc. IEEE ICASSP*, May 2006, pp. II-14–II-19.
[47] J. Oliveira, J. Bioucas-Dias, and M. Figueiredo, "Adaptive total variation image deblurring: A majorization–minimization approach," *Signal Process.*, vol. 89, no. 9, pp. 1683–1693, 2009.
[48] N. Galatsanos, "A majorization–minimization approach to total variation reconstruction of super-resolved images," in *Proc. EURASIP*, 2008, pp. 2–6.
[49] A. Chopra and H. Lian, "Total variation, adaptive total variation and nonconvex smoothly clipped absolute deviation penalty for denoising blocky images," *Pattern Recognition*, vol. 43, no. 8, pp. 2609–2619, 2010.
[50] Z. Wang, A. Bovik, and H. Sheikh, "Image quality assessment: From error visibility to structural similarity," *IEEE Trans. Image Process.*, vol. 13, no. 4, pp. 600–612, Apr. 2004.
[51] Z. Wang and A. Bovik, "Mean squared error: Love it or leave it: A new look at signal fidelity measures," *IEEE Signal Process. Mag.*, vol. 26, no. 1, pp. 98–117, Jan. 2009.
[52] L. Zhang, L. Zhang, X. Mou, and D. Zhang, "FSIM: A feature similarity index for image quality assessment," *IEEE Trans. Image Process.*, vol. 20, no. 8, pp. 2378–2386, Aug. 2011.
[53] A. Moorthy and A. Bovik, "A two-step framework for constructing blind image quality indices," *IEEE Signal Process. Lett.*, vol. 17, no. 5, pp. 513–516, May 2010.
[54] X. Zhu and P. Milanfar, "Automatic parameter selection for denoising algorithms using a no-reference measure of image content," *IEEE Trans. Image Process.*, vol. 19, no. 12, pp. 3116–3112, Dec. 2010.
[55] P. Milanfar. *MDSP Super-Resolution and Demosaicing Datasets* [Online]. Available: http://users.soe.ucsc.edu/∼milanfar/software/sr-datasets.html
[56] P. Vandewalle, S. Susstrunk, and M. Vetterli, "A frequency domain approach to registration of aliased images with application to super-resolution," *EURASIP J. Appl. Signal Process.*, vol. 2006, no. 71459, pp. 1–14, 2006.
[57] P. Vandewalle and S. Süsstrunk. *Super-Resolution Data Sets* [Online]. Available: http://lcavwww.epfl.ch/software/superresolution/index.html

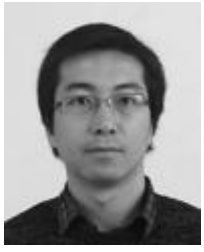

Qiangqiang Yuan received the B.S. degree in surveying and mapping engineering from Wuhan University, Wuhan, China, in 2006, where he is currently pursuing the Ph.D. degree with the State Key Laboratory of Information Engineering in Surveying, Mapping and Remote Sensing.

His current research interests include image restoration, super-resolution, and remote sensing image enhancement.

Liangpei Zhang (M'07–SM'08) received the B.S. degree in physics from Hunan Normal University, Changsha, China, in 1982, the M.S. degree in optics from the Xi'an Institute of Optics and Precision Mechanics, Chinese Academy of Sciences, Xi'an, China, in 1988, and the Ph.D. degree in photogrammetry and remote sensing from Wuhan University, Wuhan, China, in 1998.

He is currently with the State Key Laboratory of Information Engineering in Surveying, Mapping and Remote Sensing, Wuhan University, as the Head of the Remote Sensing Division. He is a Chang-Jiang Scholar Chair Professor appointed by the Ministry of Education, China. He has more than 200 research papers and 5 patents. He is a Principal Scientist for the China State Key Basic Research Project from 2011 to 2016 appointed by the Ministry of National Science and Technology of China to lead the Remote Sensing Program in China. His current research interests include hyperspectral remote sensing, high resolution remote sensing, image processing, and artificial intelligence.

Dr. Zhang regularly serves as a Co-Chair of the series SPIE Conferences on Multispectral Image Processing and Pattern Recognition, Conference on Asia Remote Sensing, and many other conferences. He edits several conference proceedings, issues, and the geoinformatics symposiums. He also serves as an Associate Editor of the *International Journal of Ambient Computing and Intelligence*, *International Journal of Image and Graphics*, *International Journal of Digital Multimedia Broadcasting*, *Journal of Geo-Spatial Information Science*, and the *Journal of Remote Sensing*. He is a fellow of IEE, an Executive Member (Board of Governor) of the China National Committee of International Geosphere-Biosphere Programme, an Executive Member for the China Society of Image and Graphics, and others.

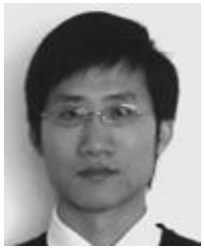

Huanfeng Shen (M'11) received the B.S. degree in surveying and mapping engineering and the Ph.D. degree in photogrammetry and remote sensing from Wuhan University, Wuhan, China, in 2002 and 2007, respectively.

In July 2007, he joined the School of Resources and Environmental Science, Wuhan University, where he is currently an Associate Professor. His current research interests include image reconstruction, remote sensing, image processing and application, data fusion, and assimilation.